Journal of Power Sources 253 (2014) 167–176

Contents lists available at ScienceDirect

Journal of Power Sources

journal homepage: www.elsevier.com/locate/jpowsour

Effects of different alkyl chains on the performance of dye-sensitized solar cells with different electrolytes

Yue Zhang [a,b], Yufeng Zhang [a], Zhihui Wang [c], Mao Liang [c,*], Dongdong Jia [c], Quanping Wu [b], Song Xue [c,*]

[a] School of Environmental Science and Engineering, Tianjin University, Tianjin 300072, China
[b] School of Electrical Engineering, Tianjin University of Technology, Tianjin 300384, China
[c] Tianjin Key Laboratory of Organic Solar Cells and Photochemical Conversion, School of Chemistry & Chemical Engineering, Tianjin University of Technology, Tianjin 300384, China

HIGHLIGHTS

- Propyl chains are better than hexyl chains in current generation in iodine cell.
- Hexyl chains are superior in suppression of charge recombination in cobalt cell.
- Electron lifetime of the cobalt cell is strongly dependent upon the alkyl chains.
- Effects of TBP on the performance of cells are also correlated to alkyl chains.
- An efficiency of 7.86% was achieved for the M24 sensitized cobalt cell.

GRAPHICAL ABSTRACT

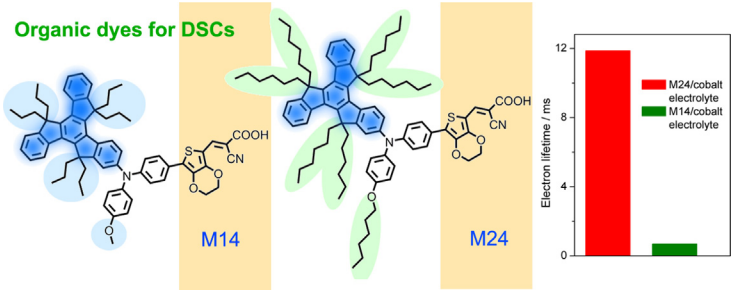

ARTICLE INFO

Article history:
Received 23 October 2013
Received in revised form
21 November 2013
Accepted 7 December 2013
Available online 18 December 2013

Keywords:
Dye-sensitized solar cell
Organic sensitizers
Alkyl chains
Electron lifetime
Photovoltaic properties
Cobalt electrolyte

ABSTRACT

To develop high-efficiency organic dyes for dye-sensitized solar cells (DSCs), a comprehensive understanding on the structure–property relationship of metal-free organic photosensitizers is warranted. To address this issue, two organic dyes (M14 and M24) featuring, respectively, propyl chains and hexyl chains have been engineered. Interestingly, it is found that the length of alkyl chains has different effects on the performance DSCs with different electrolyte (e.g., iodine electrolyte and cobalt electrolyte). Herein, we scrutinize the effects of the length of alkyl chains in terms of light-harvesting, interfacial kinetic parameters, as well as their joint contribution to the photovoltaic performance. Furthermore, the dependence of conduction band shift and electron lifetime on the concentration of 4-tert-butylpyridine (TBP) in electrolyte is also investigated.

1. Introduction

The dye-sensitized solar cell (DSC) is a promising alternative to traditional inorganic semiconductor-based solar cells because of favorable ecological and economical features [1]. Typically, a DSC comprises nano-crystalline anatase TiO_2 photoanodes adsorbed

* Corresponding authors. Tel.: +86 22 60214250.
E-mail addresses: liangmao717@126.com (M. Liang), xuesong@ustc.edu.cn (S. Xue).

0378-7753/$ – see front matter © 2013 Elsevier B.V. All rights reserved.
http://dx.doi.org/10.1016/j.jpowsour.2013.12.032

with a sensitizer, an iodide/triiodide redox couple as the electrolyte, and a conductive glass coated with platinum as the cathode [2]. The sensitizer, which acts as the light harvesting antennae, is essential for efficient light harvesting and electron generation/transfer. During the past two decades, numerous research attempts have been made to explore new photosensitizers in the development of DSCs [3–15]. Amongst these emerging photosensitizers, arylamine organic sensitizers with robust availability, ease of structural tuning and generally high molar extinction coefficient, have recently received great attention [16].

In the fabrication of high-efficiency DSCs, the iodine electron mediator has so far served as a very successful option owing to an expeditious electron donation from iodide to some photo-oxidized dye molecules, a sluggish recombination of photo-injected electrons in titania with triiodide, and a rapid mass transport of redox ions in a thin-layer sandwich device architecture [17]. One of the main drawbacks with the iodide/triiodide redox couple is, however, the large driving force needed for the dye regeneration [18–20]. Therefore, alternative redox couples, such as cobalt(II/III) redox shuttle, have been explored for DSCs to avoid the problem mentioned above [21].

The combination of some cobalt redox shuttles with organic dyes has recently brought forth a new opportunity towards efficiency enhancement of DSCs [22]. For instance, DSCs based on C220 [23], C235 [23] and JF419 [24] achieve an excellent power conversion efficiency of over 10% at AM 1.5G simulated sunlight (100 mW cm^{-2}) in the presence of a standard cobalt electrolyte. Very recently, based upon the chromophoric core of cyclopentadithiophene–benzothiadiazole, Wang and co-workers have finely tailored a metal-free organic dye (C259) which displays power conversion efficiencies of 11.5–12.8% under various irradiances of the simulated air mass (AM) 1.5 sunlight, setting a new benchmark for the cobalt cells [4b]. Evidently, the use of a cobalt redox shuttle can confer a salient V_{OC} enhancement. However, this does not mean high efficiency DSCs could be obtained by simply replacing the iodide/triiodide couple with cobalt redox couple. As a matter of fact, it has been found that the same organic dye may exhibit quite different structure–property relationship in cobalt control cells compared with that in iodine control cells [25,26]. These studies indicate that the structure–property relationship of organic dyes in cobalt cells needs to be systematically investigated, which is pivotal for exploring high efficiency organic dyes for cobalt control cells.

In this work, we focus on the effects of alkyl chains length of organic dyes on photovoltaic performances of DSCs employing an iodine or cobalt electrolyte. To the best of our knowledge, there have been surprisingly few investigations on this issue. Herein, we employ two truxene organic dyes (M14 and M24, their molecular structures are illustrated in Fig. 1.) with different linear propyl and hexyl chains, respectively, to carry out this interesting investigation. Effects of hydrocarbon chains length on photovoltaic performance of DSCs employing different electrolyte are scrutinized in terms of light-harvesting, interfacial kinetic parameters, as well as their joint contribution to photovoltaic performance. Our work provides an important new insight into the structure–property relationship of organic dyes for DSCs employing the cobalt(II/III) redox shuttle.

2. Results and discussion

The synthetic procedure for M24 is depicted in Scheme 1. Monosubstituted truxene bromide **1** was reacted with 4-(hexyloxy)-*N*-phenylaniline (**2**) in the presence of potassium *tert*-butoxide, palladium acetate and tri-*tert*-butylphosphine to give **3**. Compound **5** was obtained by a bromination reaction and Suzuki coupling. Aldehyde **6** was synthesized by a Vilsmeier–Haack reaction of **5** with $POCl_3$ and DMF. Subsequently, the target dye M24 was obtained via Knoevenagel condensation reaction of the aldehyde **6** with cyanoacetic acid in the presence of a catalytic amount of piperidine. All the intermediates and target dyes were characterized by standard spectroscopic methods. The synthesis of M14 dye has been reported in our previous publication [25].

2.1. Absorption spectra

UV/Vis absorption spectra of the resulting dyes in a diluted solution of CH_2Cl_2 are shown in Fig. 2a and the corresponding photophysical data are summarized in Table 1. Both of the two dyes have a relatively broad and strong absorption in ultraviolet and visible regions. The absorption band at 350–400 nm can be ascribed to the π–π^* transitions of the conjugated system, while the band in the range of 430–600 nm mainly stems from the intramolecular charge-transfer transition (ICT) between donor and acceptor. The major absorption peaks for M14 and M24 are at 360/523 and 361/527 nm, respectively. Compared with M14, a bathochromic shift of 4 nm can be found for M24. This may be attributed to stronger ability of donating electron of hexyloxybenzene in comparison with methoxybenzene, which enhances the donor strength of the amine segment to result in a pronounced donor–acceptor interaction [27]. It is also found that, consistent with other studies [27], the introduction of long alkyl chains at the end of the molecule evokes a reduced molar extinction coefficient. In spite of that, M14 and M24 both have high molar extinction coefficients (over 58 900 M^{-1} cm^{-1}), leading to excellent light harvesting. They are therefore convenient sensitizers for DSCs based on the cobalt(II/III) redox shuttle, where thinner TiO_2 film is preferred to overcome mass transport and recombination limitations associated with the polypyridyl cobalt redox shuttles [28].

Fig. 3 displays the absorption spectra of the dyes anchored on transparent mesoporous titania films (3 μm). The absorption maxima of M14 and M24 lie in 472 and 482 nm, respectively. In comparison with their absorption maxima in solution, a

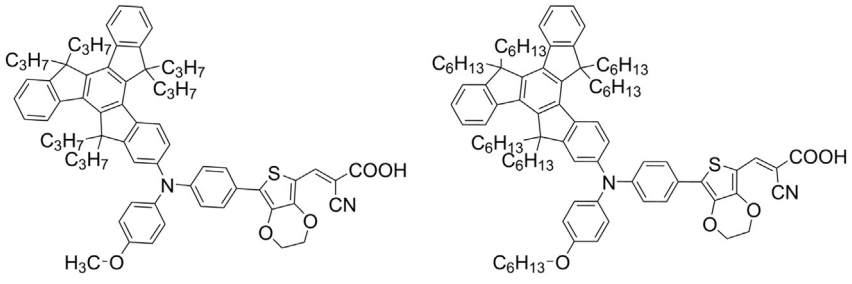

Fig. 1. Chemical structures of M14 and M24.

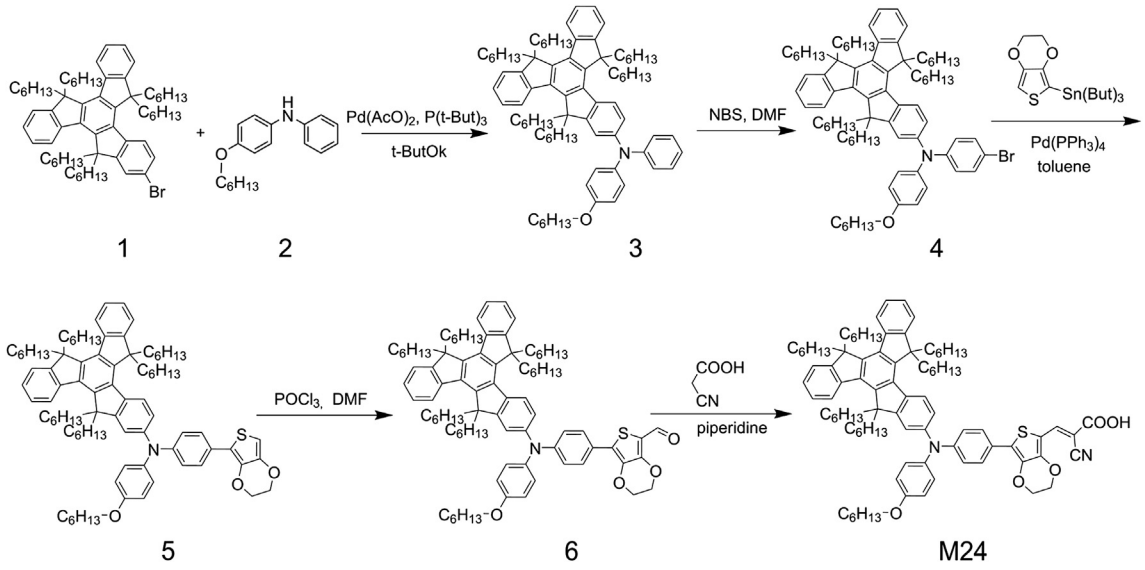

Scheme 1. Synthetic route for M24.

hypsochromic shift of 51 and 45 nm can be observed for M14 and M24, respectively. Such a hypsochromic shift can be attributed to the deprotonation of carboxylic acid, a result that has been observed for other metal-free organic dyes.

2.2. Electrochemical properties

Cyclic voltammetry was conducted in acetonitrile solution to verify whether the ground and excited oxidation potentials of M14 and M24 are suitable for fabrication of DSCs (Fig. 4). As shown in Table 1, the first oxidation potentials ($E_{D/D+}$) of M14 and M24, corresponding to the HOMO level of dyes, are more than 600 mV positive than I^-/I_3^- redox couples (400 mV vs NHE), indicating the driving forces for dye regeneration are sufficient for the iodine control cells. In contrast to the large driving forces in iodine cells, the driving forces for dye regeneration in cobalt cells (e.g., $Co^{II/III}$-tris(phen) hexafluorophosphate couple, 620 mV vs NHE [25]) are generally small, being 400 and 380 mV for M14 and M24, respectively. Note that, the values are much higher than that of an early reported truxene-based dye, M16 (280 mV) [26]. It can be expected that the driving forces for M14 and M24 in cobalt control cells are sufficient to regenerate most of M14 and M24.

The excited-state potential ($E_{D^*/D+}$), reflecting the LUMO level of the dyes, can be derived from the ground-state oxidation potential and the zero–zero excitation energy (E_{0-0}) determined from the intersection of absorption and emission spectra (Fig. 2b). The LUMO of M14 and M24 are calculated to be −1.13 and −1.15 V, respectively, indicative of thermodynamic feasibility for electron injection to conduction band (E_{CB}) of TiO_2 (−0.5 V versus NHE).

2.3. Computational analysis

To gain insight into the geometrical and electronic properties of the resulted sensitizers, DFT calculations and time-dependent DFT

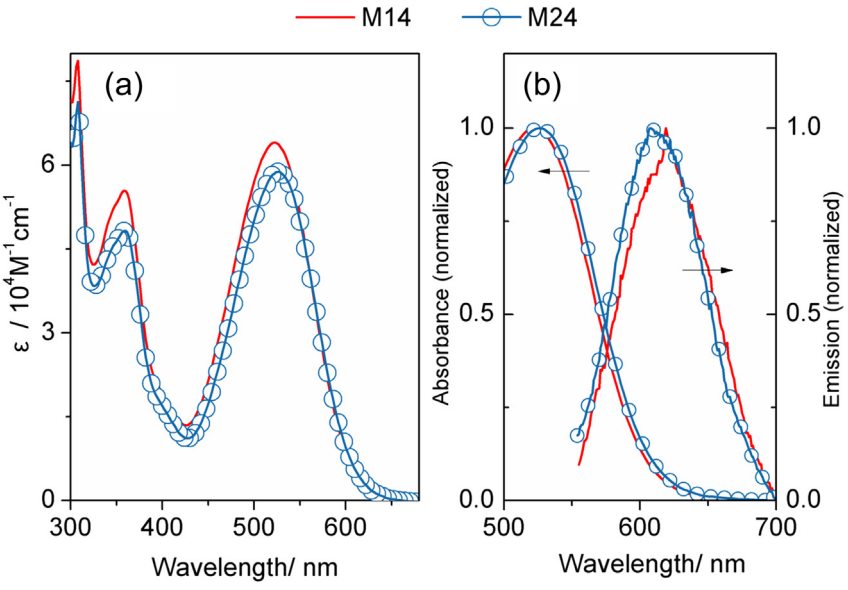

Fig. 2. Absorption (a) and emission (b) spectra of the M14 and M24.

Table 1
Photophysical and electrochemical data for the dyes.

Dye	λ_{max}[a]/nm (ε/10^3M^{-1} cm^{-1})	E_{0-0}/eV	$E_{D/D+}$[b]/V	$E_{D^*/D+}$[c]/V
M14	360 (55.3), 523 (63.8)	2.15	1.02	−1.13
M24	361 (48.2), 527 (58.9)	2.15	1.00	−1.15

[a] The absorption spectra were measured in CH_2Cl_2 solutions.
[b] The $E_{D/D+}$ (vs NHE) were measured in acetonitrile.
[c] $E_{D^*/D+}$ were estimated from calculated from $E_{D^*/D+} = E_{ox} - E_{0-0}$.

(TDDFT) calculations of the excited states were performed. We optimized the molecular structure of M14 and M24 in the vacuo, and the isodensity surface plots of HOMO and LUMO are presented in Fig. 5. The HOMO orbital of M14/M24 is delocalized over the entire molecule with maximum components on the truxene-based triarylamine. The LUMO orbital is, on the other hand, a single π^* orbital delocalized across the EDOT spacer and cyanoacrylic acid groups with sizable contributions from the latter. The results indicate that the electrons in the donor could be successively transferred to the acceptor part and then injected into the conduction band of TiO_2 after being illuminated by the light.

2.4. Photovoltaic performance of DSCs

Action spectra of the incident photon-to-current conversion efficiencies (IPCE) as a function of incident wavelength for the cobalt cells based on the resulting organic dyes are shown in Fig. 6. Electrolyte E1 was composed of 0.25 M $[Co(II)(phen)_3](PF_6)_2$, 0.05 M $[Co(III)(phen)_3](PF_6)_3$, 0.3 M TBP and 0.1 M LiTFSI in acetonitrile. E2 was identical to E1 though with 0.8 M TBP. Regardless of the electrolyte section, the IPCE spectra for DSCs based on M24 are broader than those for M14, which are in good agreement with their absorption properties. The highest IPCE values of 85.5 and 83.1% are achieved for M14 and M24 sensitized cells employing the E1 electrolyte, respectively. Note that, alteration of the cobalt electrolyte from E1 to E2 decreases $IPCE_{max}$ from 85.5 to 79.5%. In contrast, the $IPCE_{max}$ variation correlated with electrolyte for M24 sensitized cells is very small. To comprehend the IPCE variation, factors contributing to IPCE need to be considered. As we have known, IPCE is expressed by the product of light harvesting efficiency (LHE) and absorbed photon-to-current conversion efficiency (APCE) [29]:

$$IPCE(\lambda) = LHE \times APCE = LHE \times \eta_{col} \times \eta_{inj}$$

where APCE can be divided into two terms: the overall charge collective efficiency (η_{col}) and the overall electron injection efficiency (η_{inj}). Clearly, the LHE would not change for the cells based on the same dye. Therefore, any difference in the photocurrent could be attributed to the difference of η_{col} and η_{inj}. As shown in Fig. 6, the influences of TBP concentration variation on APCE of M14 sensitized cells is more pronounced than those of M24. This interesting result will be discussed in detail in the following sections.

We further recorded the photocurrent–voltage (J–V) characteristics (Fig. 7) of DSCs employing the E1 and E2 electrolytes to evaluate the effects of different alkyl chains on photovoltaic parameters. The detailed photovoltaic parameters are summarized in Table 2. A relatively thin titania film (3 μm) is employed so as to avoid the mass transport limitation of the cobalt(II/III) redox shuttle and to minimize interfacial charge recombination. The short-circuit photocurrent density (J_{SC}), open-circuit photovoltage (V_{OC}) and fill factor (FF) of M14 cells employing the E2 electrolyte are 10.7 mA cm^{-2}, 846 mV and 0.71, respectively, affording an overall power conversion efficiency (PCE) of 6.42%. By comparison, the introduction of longer alkyl chains in M24 significantly increased V_{OC} for about 100 mV, contributing to an evidently enhanced PCE of 7.86%. Note that, a significant improvement of cell efficiency can be noticed for the M24 sensitized cells with the cobalt electrolyte in comparison with those of M14, indicating that long alkyl chains are better than short alkyl chains in terms of the photovoltaic performance of the cobalt cells.

In contrast to the cobalt cells, the influences of the length of alkyl chain on the photovoltaic performance of the iodine cells are different. The J–V curves of the devices measured under AM 1.5 irradiation (100 mW cm^{-2}) are shown in Fig. 8, and the detailed photovoltaic parameters are summarized in Table 3. M14 sensitized iodine cells showed only a 12–21 mV decrease of V_{OC} as compared to those of the M24 sensitized cells. It is noteworthy that, the J_{SC} of M14 sensitized cells are higher than those of the M24 sensitized cells, contrasting a slight decrease of photocurrents in cobalt cells. In order to clarify the physical origins of the J_{SC} variation, we estimated the amounts of the dyes adsorbed on the TiO_2 surface by desorbing the dyes with a 0.01 M solution of KOH in methanol. The surface concentrations were determined to be 0.86 × 10^{-7} and 0.70 × 10^{-7} mol cm^{-2} for M14 and M24, respectively. Higher amounts of M14 due to smaller size cause an enhanced photocurrent in the iodine cells, while the enhanced charge recombination

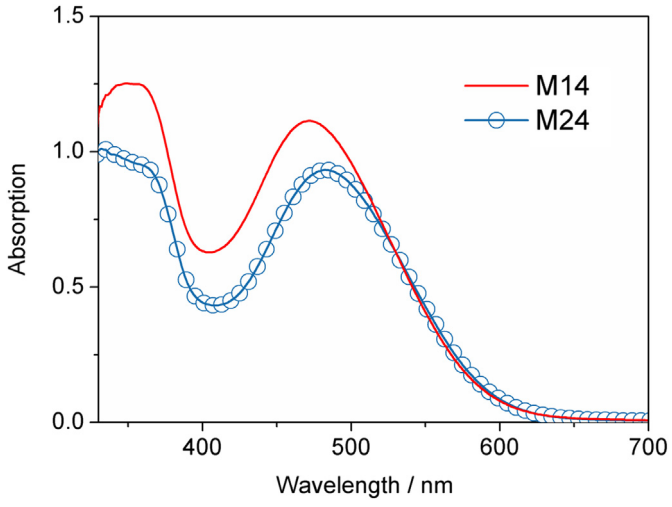

Fig. 3. Absorption spectra of sensitized electrodes based on M14 and M24.

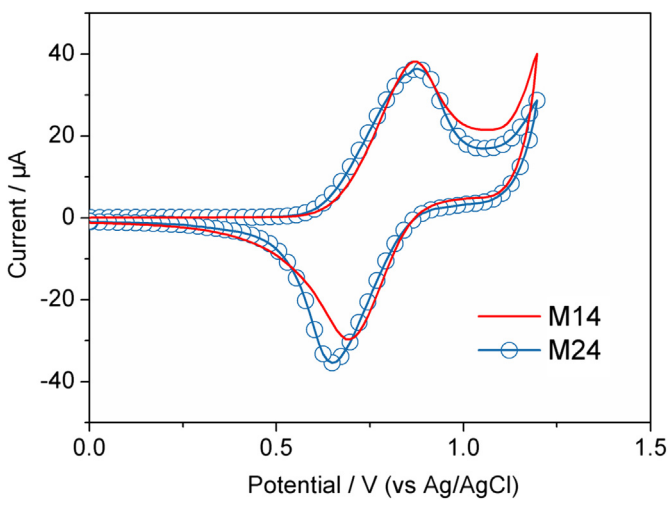

Fig. 4. CV lines of sensitized electrodes based on M14 and M24.

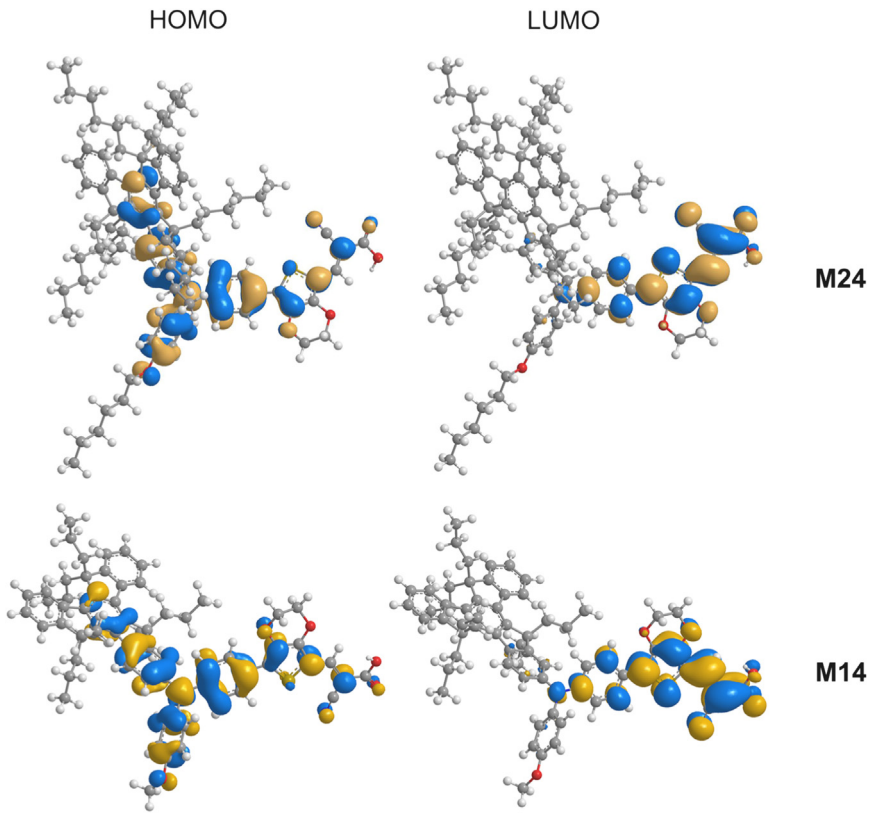

Fig. 5. Computed frontier orbitals of M14 and M24.

at the semiconductor/dye/electrolyte interface in cobalt cells should be partially responsible for the lower J_{SC} of M14 (see following section). As a result, the photovoltaic performances of the iodine cells based on M14 are superior to those of M24, contrasting the results observed for the cobalt cells. M14 and M24 sensitized DSCs with the E3 electrolyte produced J_{SC} of 11.2 and 10.2 mA cm^{-2}, V_{OC} of 745 and 766 mV, and *FF* of 0.68 and 0.69, corresponding to PCEs of 5.67 and 5.39%, respectively. From the photovoltaic measurements, it is clear that the length of alkyl chains in the organic dyes has a different effect on the performance of DSCs employing different electrolytes.

2.5. Dependence of the conduction band shift and electron lifetime on the electrolytes containing different concentration of TBP

It is noted that, the electrolyte selection has caused some interesting results which is intimately correlated with the length of alkyl chains. To scrutinize the origin of the photovoltaic parameters variation, dependence of the conduction band (CB) shift and electron lifetime on the electrolytes was investigated. In this work, charge densities at open-circuit, measured by charge extraction technique under illumination of a green light from LED [30], were used to compare the conduction band positions in different DSCs. The electron lifetime (τ) at open circuit, measured by controlled

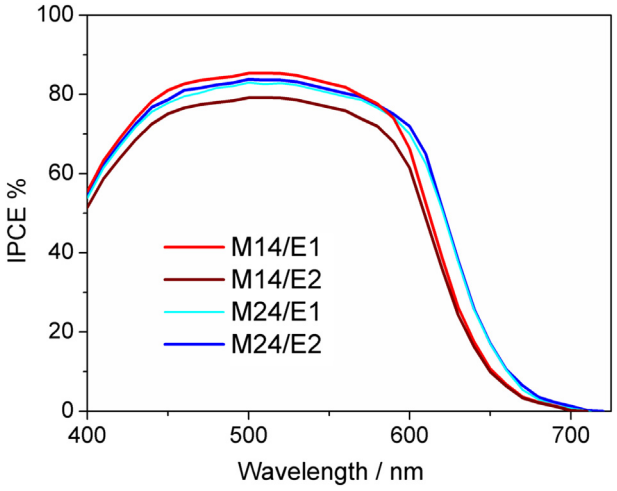

Fig. 6. IPCE spectra of the DSCs employing the cobalt electrolytes.

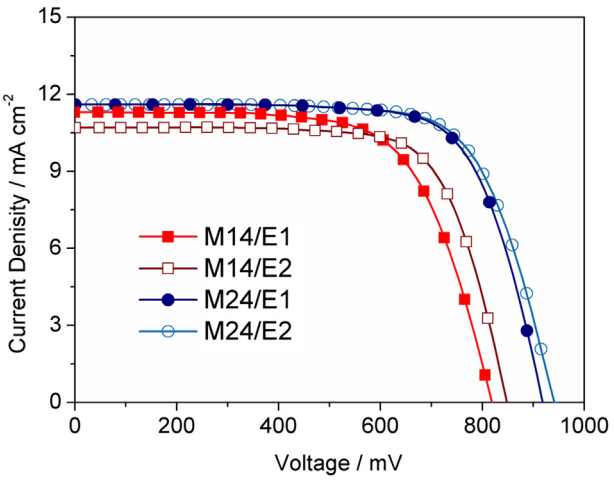

Fig. 7. *J*–*V* curves of the DSCs employing the cobalt electrolytes.

Table 2
Photovoltaic parameters of the DSCs employing the cobalt electrolytes.[a]

Dye/electrolyte	J_{SC}/mA cm^{-2}	V_{OC}/mV	*FF*	PCE/%
M14/E1	11.3	819	0.69	6.38
M14/E2	10.7	846	0.71	6.42
M24/E1	11.6	916	0.71	7.54
M24/E2	11.6	942	0.72	7.86

[a] Measurements were performed under AM 1.5 irradiation. Electrolyte E1: 0.25 M [Co(II)(phen)$_3$](PF$_6$)$_2$, 0.05 M [Co(III) (phen)$_3$](PF$_6$)$_3$, 0.3 M TBP and 0.1 M LiTFSI in acetonitrile. E2 was identical to E1 though with 0.8 M TBP.

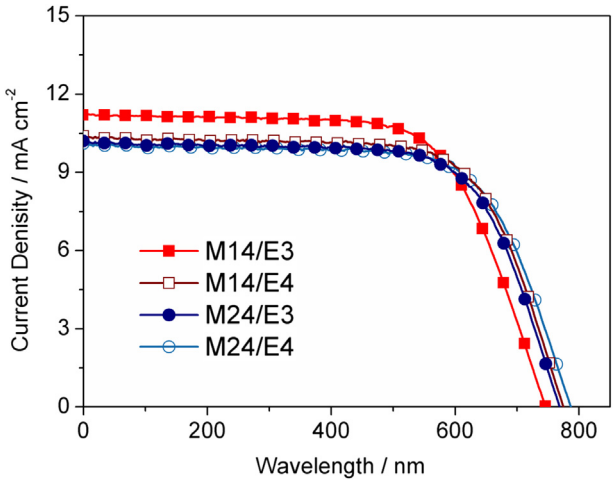

Fig. 8. *J*–*V* curves of DSCs employing the iodine electrolytes.

intensity modulated photovoltage spectroscopy (IMVS), can be obtained by fitting either the real or imaginary part of the IMVS response (Eqs. (1) and (2)) [31].

$$\mathrm{re}(\Delta V_{OC}) = \frac{X_1}{1+(\omega\tau^{re})^2} \quad (1)$$

$$\mathrm{im}(\Delta V_{OC}) = -\frac{X_2\omega\tau^{im}}{1+(\omega\tau^{im})^2} \quad (2)$$

where im(ΔV_{OC}) is the imaginary modulation of the photopotential (ΔV_{OC}), re(ΔV_{OC}) is the real modulation of the photopotential (ΔV_{OC}), X_1, X_2, τ^{re} and τ^{im} are the fit parameters, ω is the circular frequency of the light modulation.

Fig. 9 shows the relation between V_{OC} and extracted charge density (*Q*) at open circuit. The curves for M14 and M24 sensitized cells are roughly parallel to each other. At a fixed *Q*, a higher V_{OC} value indicates a negative shift of the CB, while a decreased V_{OC} means a positive shift of the CB. According to the Q–V_{OC} plots, regardless of electrolyte selection, the M14 cells showed an upward CB shifts over 20 mV as compared to the M24 cells. Evidently, the CBs of the M14 cells are higher than those of the M24 cells with the same electrolyte. As a result, the driving forces of the M14 cells for the electron injection are lower than those of the M24 cells. On the other hand, it can be found that, for all the cells, the presence of 0.8 M TBP caused the TiO_2 bands to be shifted upward as compared to that of 0.3 M TBP, leading to a decrease of the driving forces for the electron injection. Recent study has shown that it is possible for an insufficient driving force for electron injection to induce poor η_{inj} [32]. However, the relatively lower driving forces of the M14 cells could not be the only reason for the profound influence of TBP concentration on the APCE of the M14 sensitized cells as mentioned above.

Fig. 10 shows the electron lifetime as a function of *Q* for the M14 and M24 cells. It was found that, regardless of the electrolyte selection, the electron lifetime increased with the increasing concentration of TBP, indicating that charge recombination between electrons in the TiO_2 film and Co(III) ions in the electrolyte are retarded by the addition of TBP. The retardation of charge recombination at the titania/electrolyte interface by increasing the TBP content of the electrolyte leads to an increased η_{col} for all cells. Nevertheless, when carefully comparing the TBP correlated electrolyte lifetime variation for the dyes, a distinct difference is observed. For example, it can be found that the electrolyte alteration from E3 to E4 has caused a 1.7-fold increase of electrolyte lifetime for the M24 cells. In contrast, the electrolyte lifetime of M14 sensitized cell with the E4 electrolyte is only slightly higher than that of the corresponding cell with the E3 electrolyte, indicating a slightly improved η_{col}.

Taking these results into consideration, it is possible that the positive effect of the η_{col} enhancement could not compensate the adverse impact of the attenuated driving force for electron injection, thus resulting in a decreased J_{SC} for M14 sensitized cell with the E4 electrolyte. In contrast, for M24 sensitized cells, there seems to be a balance between increased η_{col} and attenuated η_{inj} with the increase of TBP concentrations. Not surprisingly, M24 sensitized cell with E4 electrolyte provides a comparable J_{SC} as compared to the corresponding cell with E3 electrolyte. $IPCE_{max}$ variation correlated with E1/E2 electrolyte mentioned above could be ascribed to the same reason.

Furthermore, it is noteworthy that, the dependence of electron lifetime on the electrolyte is different for M14 and M24. As presents in Fig. 10, the dye alteration from M14 to M24 has caused a 17.0-fold increased electron lifetime, accounting for the significantly increased V_{OC} as well as higher J_{SC} observed for the cells with E2 electrolyte. In contrast, for the iodine cells (e.g., E4 electrolyte), the

Table 3
Photovoltaic parameters of the DSCs employing the iodine electrolytes.[a]

Dye/electrolyte	J_{SC}/mA cm^{-2}	V_{OC}/mV	*FF*	PCE/%
M14/E3	11.2	745	0.68	5.67
M14/E4	10.4	772	0.69	5.54
M24/E3	10.2	766	0.69	5.39
M24/E4	10.1	784	0.69	5.46

[a] Measurements were performed under AM 1.5 irradiation. Electrolyte E3, 0.25 M 1,2-dimethyl-3-n-propylimidazolium iodide (DMPIml), 0.1 M LiTFSI, 0.05 M I_2, and 0.3 M TBP in acetonitrile. E4 was identical to E3 though with 0.8 M TBP.

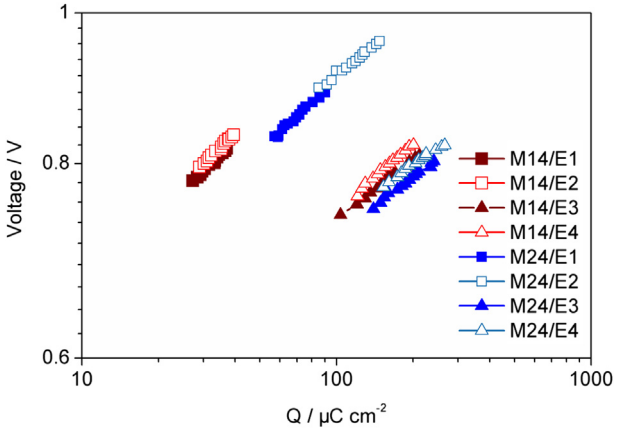

Fig. 9. Open circuit as a function of charge density for the studied DSCs.

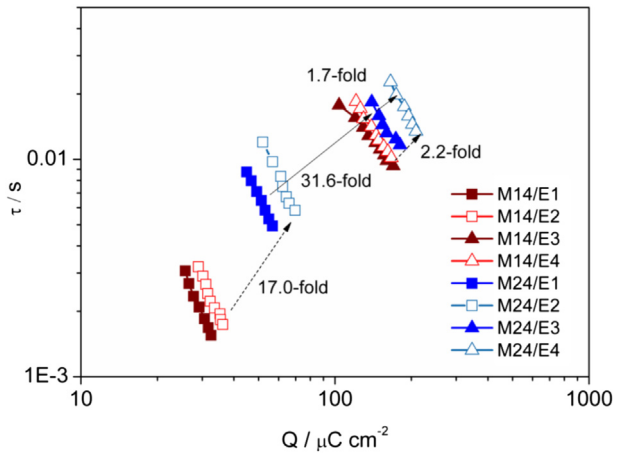

Fig. 10. Electron lifetime as a function of charge density for the studied DSCs.

electron lifetime of M24 sensitized cell is only 2.2-fold higher than that of M14 sensitized cell. This observation intimately correlates to the intrinsic properties of electrolytes. Note that, the $[Co(III)(phen)_3]^{3+}$ ion is more bulky than the I_3^- ion. The ionic diameter of I_3^- is about 5.3 Å (determined by the ChemBio3D ultra 11.0 program), while the $[Co(III)(phen)_3]^{3+}$ ion is a sphere with diameter of about 12.1 Å (determined by the ChemBio3D ultra 11.0 program). With respect to the $[Co(III)(phen)_3]^{3+}$ ions, the small I_3^- ions would be more easily to penetrate a M24 dye layer. This is thought to be the main reason for the fact that the M24 is less efficient in blocking the I_3^- ions as compared to the $[Co(III)(phen)_3]^{3+}$ ions.

The superiority of M24 with long alkyl chains regarding reduction of charge recombination can be understood from molecular modeling studies of M14 and M24. As illustrated in Fig. 11, M24 has a bulkier structure than that of M14, especially regarding the top view of the molecule. M24 provides a considerably large "protected" area, approximated 449.7 $Å^2$, while that of M14 lies in 185.7 $Å^2$. The bulky structure of M24 can readily block the Co(III) ions in the cobalt electrolyte approaching the TiO_2 surface, thereby suppressing electron recombination.

3. Conclusions

To summarize, based on M14 and M24, we have investigated some general impacts of the length of alkyl chains on the optoelectronic features of DSCs employing the iodine and cobalt electrolytes. We found that length of alkyl chains on the organic dyes has different effects on the performance of DSCs with the cobalt electrolyte and the iodine electrolyte. In conjunction with the iodine electrolyte, M14 dye containing propyl chains exhibits better J_{SC} and thus PCE than M24 featuring hexyl chains due to higher amounts of dyes adsorbed and comparable electron lifetime. In contrast, the performances of M24 sensitized cobalt cells are superior to those of M14 benefiting from significantly improved electron lifetime. IMVS data have revealed that the electron lifetime of the cobalt cells are strongly dependent upon the length of alkyl chains, while the electron lifetime of the iodine cells are found to be only weakly dependent upon the length of alkyl chains. Interestingly, the charge density and electron lifetime data have demonstrated that the dependence of photovoltaic performance of cells on the TBP concentration is also correlated with the length of alkyl chains. The J_{SC} of the M14 sensitized cells decreased with increasing TBP concentration, while no significant change in J_{SC} was observed for M24. From our finding, we proposed that organic dyes with long alkyl chains in donor part should be preferred in the future development of organic sensitizers for iodine-free DSCs.

4. Experimental

4.1. Materials and instruments

The synthetic route for M24 is shown in Scheme 1. *n*-Butyllithium, $Pd(PPh_3)_4$, $Pd(OAc)_2$, $SnBu_3Cl$, *t*-BuOK, $(t\text{-}Bu)_3P$ and cyanocertic acid were purchased from Energy Chemical (China). 4-*Tert*-pyridine (TBP) and 0.1 M Lithium bis(trifluoromethanesulfonyl) imide (LiTFSI) were purchased from Aldrich. *N*,*N*-Dimethylformamide was dried over and distilled from CaH_2 under an atmosphere

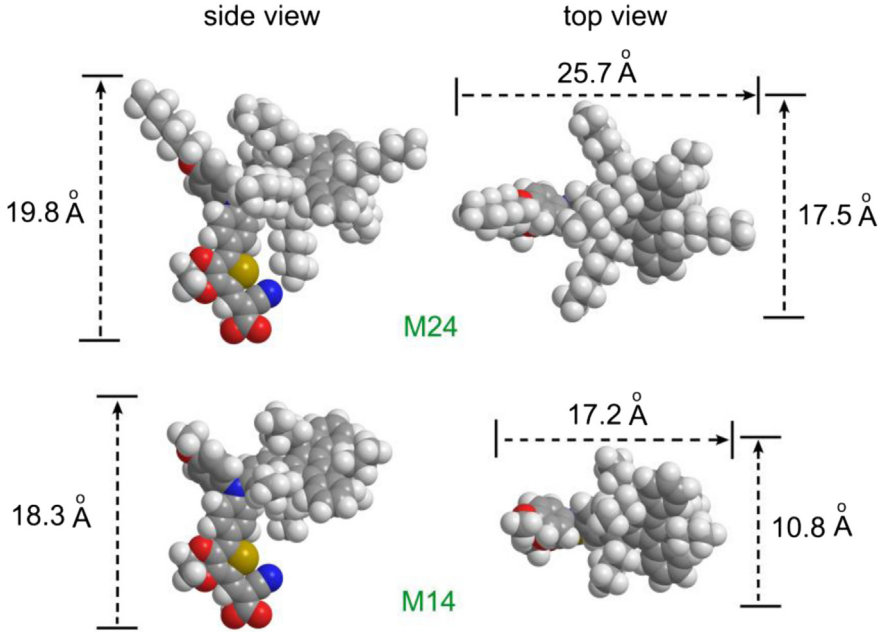

Fig. 11. Molecular structures of M14 and M24 derived from density functional theory (DFT) calculations (b3lyp).

of nitrogen. Phosphorus oxychloride was freshly distilled before use. Dichloromethane was distilled from calcium hydride under nitrogen atmosphere. All other solvents and chemicals used in this work were analytical grade without further purification. Melting points of the samples were taken on an RY-1 melting point apparatus (Tianfen, China). ^{1}H NMR and ^{13}C NMR spectra were recorded on a Bruker AM–400 spectrometer. The reported chemical shifts were against TMS. High resolution mass spectra were obtained with a Micromass GCT-TOF mass spectrometer.

4.2. Photophysical and electrochemical measurements

The absorption spectra of the dyes were measured by SHIMADZU UV-2600 spectrophotometer. Fluorescence measurements were carried out with a HITACHI F-4500 fluorescence spectrophotometer. FT-IR spectra were obtained with a Bio-Rad FTS 135 FT-IR instrument.

Cyclic voltammetry (CV) measurements for the dyes sensitized films were performed on a Zennium electrochemical workstation (ZAHNER), with sensitized electrodes as the working electrode, Pt-wires as the counter electrode, and an Ag/AgCl electrode as the reference electrode at a scan rate of 50 mV s^{-1}. Tetrabutylammonium perchlorate (TBAP, 0.1 M) and MeCN were used as supporting electrolyte and solvent, respectively. The measurements were calibrated using ferrocene as standard. The redox potential of ferrocene internal reference is taken as 0.63 V vs NHE.

4.3. Fabrication and characterization of DSCs

The TiO_2 paste (particle size, 20 nm) was printed on a conducting glass (Nippon Sheet Glass, Hyogo, Japan, fluorine-doped SnO_2 over layer, sheet resistance of 10 Ω sq^{-1}) using a screen printing technique. The film was dried in air at 120 °C for 30 min and calcined at 500 °C for 30 min under flowing oxygen before cooling to room temperature. The heated electrodes were impregnated with a 0.05 M titanium tetrachloride solution in a water-saturated desiccator at 70 °C for 30 min and fired again to give a ca. 3 μm thick mesoscopic TiO_2 film. The TiO_2 electrode was stained by immersing it into a 0.3 mM dye solution in a mixture of DCM/EtOH (v/v, 1:1) and kept at room temperature for 24 h to complete the sensitizer uptake. Then the sensitized electrodes were rinsed with dry ethanol and dried by a dry air flow. Pt catalyst was deposited on the FTO glass by coating with a drop of H_2PtCl_6 solution (40 mM in ethanol) with the heat treatment at 395 °C for 15 min to give photoanode. The sensitized electrode and Pt-counter electrode were assembled into a sandwich type cell by a 25 μm-thick Surlyn (DuPont) hot-melt gasket and sealed up by heating. Electrolyte E1: 0.25 M $[Co(II)(phen)_3](PF_6)_2$, 0.05 M $[Co(III)(phen)_3](PF_6)_3$, 0.3 M TBP and 0.1 M LiTFSI in acetonitrile. E2 was identical to E1 though with 0.8 M TBP. Electrolyte E3, 0.25 M 1,2-dimethyl-3-n-propylimidazolium iodide (DMPImI), 0.1 M LiTFSI, 0.05 M I_2, and 0.3 M TBP in acetonitrile. E4 was identical to E3 though with 0.8 M TBP.

The photocurrent–voltage (J–V) characteristics of the solar cells were carried out using a Keithley 2400 digital source meter controlled by a computer and a standard AM 1.5 solar simulator–Oriel 91160–1000 (300 W) SOLAR SIMULATOR 2 × 2 BEAM. The light intensity was calibrated by an Oriel reference solar cell. A metal mask with an aperture area of 0.2 cm^2 was covered on a testing cell during all measurements. The action spectra of monochromatic incident photon-to-current conversion efficiency (IPCE) for solar cell were performed by using a commercial setup (QTest Station 2000 IPCE Measurement System, CROWNTECH, USA).

Charge densities at open circuit and intensity modulated photovoltage spectroscopy (IMVS) were performed on a Zennium electrochemical workstation (ZAHNER, Germany), which includes a green light-emitting diode (LED, 532 nm) and the corresponding control system. The intensity-modulated spectra were measured at room temperature with light intensity ranging from 5 to 75 W m^{-2}, in modulation frequency ranging from 0.1 Hz to 10 kHz, and with modulation amplitude less than 5% of the light intensity.

4.4. The detailed experimental procedures and characterization data

4.4.1. Synthesis of compound **2**

Into a 250 mL two neck round-bottom flask was added compound **1** (9.26 g, 10 mmol), *N*-((4-methyloxy)phenyl)benzenamine (3.49 g, 13 mmol), $Pd(AcO)_2$ (225 mg, 1 mmol), P(*t*-But)$_3$ (1.4 mL), *t*-BuOK (1.68 g, 15 mmol) and 40 mL toluene. The reaction mixture was refluxed overnight under nitrogen. After cooling to room temperature, saturated NH_4Cl was added and extracted with ethyl acetate (3 × 10 mL). The combined organic layers were washed with brine and then dried over anhydrous magnesium sulfate, filtered, and concentrated in vacuo to give the crude product, which were purified by column chromatograph packed with silica gel using petroleum ether/ethyl acetate (10:1) as eluent to afford a light-yellow oil (5.79 g, 52% yield). IR (KBr): 2956, 2924, 2856, 1594, 1506, 1470, 1240, 749 cm^{-1}. ^{1}H NMR (400 MHz, $CDCl_3$): δ 8.40 (d, J = 7.6 Hz, 1H), 8.34 (d, J = 7.4 Hz, 1H), 8.21 (d, J = 8.6 Hz, 1H), 7.50–7.47 (m, 2H), 7.44–7.36 (m, 4H), 7.31–7.20 (m, 7H), 7.03–7.02 (m, 2H), 6.92 (d, J = 8.8 Hz, 2H), 3.97 (t, J = 6.5 Hz, 2H), 3.03–2.89 (m, 6H), 2.16–2.02 (m, 4H), 1.97–1.89 (m, 2H), 1.44–1.39 (m, 4H), 1.05–0.83 (m, 42H), 0.72–0.52 (m, 31H). ^{13}C NMR (100 MHz, $CDCl_3$): δ 155.8, 155.7, 153.6, 153.6, 155.0, 144.6, 140.8, 140.7, 140.5, 140.4, 138.2, 129.0, 127.1, 127.0, 126.2, 126.0, 125.9, 125.4, 125.2, 124.6, 122.8, 122.7, 122.2, 121.8, 121.6, 121.1, 121.0, 120.5, 116.8, 115.4, 68.3, 55.9, 55.7, 55.6, 55.5, 37.0, 36.8, 36.6, 31.6, 31.5, 31.4, 29.5, 29.4, 29.3, 25.8, 24.0, 23.9, 23.8, 22.6, 22.3, 22.2, 14.0, 13.9, 13.8. HRMS (ESI) calcd for $C_{81}H_{111}NO$ ($M + H^+$): 1114.8744, found: 1114.8717.

4.4.2. Synthesis of compound **3**

To a stirred solution of compound **2** (1.91 g, 1.72 mmol) in DMF (10 mL) was added dropwisely a solution of *N*-bromosuccinimide (NBS, 337 mg, 1.89 mmol) dissolved in dimethylformamide (DMF, 5 mL) at room temperature. The mixture was stirred overnight in dark. Ice water was added to terminate the reaction and the product was extracted with ethyl acetate. The combined organic layers were washed with brine water and dried with anhydrous $MgSO_4$. The solvent was evaporated in vacuo and the remaining crude product was purified by column chromatography with silica gel using petroleum ether/dichloromethane (10:1) as eluent to give a light yellow oil (1.72 g, 84% yield). IR (KBr): 2956, 2924, 2855, 1506, 1485, 1241 cm^{-1}. ^{1}H NMR (400 MHz, $CDCl_3$): δ 8.36–8.13 (m, 3H), 7.56–7.32 (m, 8H), 7.13–6.99 (m, 6H), 6.88 (d, J = 8.8 Hz, 2H), 3.97 (t, J = 6.5 Hz, 2H), 2.98–2.73 (m, 6H), 2.10–1.96 (m, 4H), 1.82–1.79 (m, 2H), 1.40–1.35 (m, 4H), 0.98–0.85 (m, 42H), 0.68–0.49 (m, 31H). ^{13}C NMR (100 MHz, $CDCl_3$): δ 156.1, 156.0, 155.2, 155.0, 153.6, 153.5, 153.4, 147.5, 146.2, 146.0, 144.6, 144.2, 144.1, 143.7, 143.6, 140.4, 140.3, 140.1, 139.5, 139.4, 138.5, 138.4, 138.2, 137.3, 137.2, 132.4, 132.0, 129.1, 127.2, 126.5, 126.3, 126.1, 126.0, 125.9, 125.4, 124.6, 123.9, 123.8, 122.2, 122.1, 121.2, 120.6, 117.0, 116.8, 115.4, 68.3, 55.9, 55.8, 55.7, 55.6, 55.5, 37.0, 36.9, 36.8, 36.7, 31.6, 31.5, 31.4, 29.5, 29.4, 29.3, 25.8, 24.0, 23.9, 23.8, 22.6, 22.3, 14.1, 14.0, 13.9, 13.7. HRMS (ESI) calcd for $C_{81}H_{110}NOBr$ ($M + H^+$): 1194.7854, found: 1194.7832.

4.4.3. Synthesis of compound **5**

To a 50 mL two-neck round-bottom flask, $Pd(PPh_3)_4$ (60 mg), compound of **3** (1.19 g, 1 mmol), compound **4** (517 mg, 1.20 mmol)

and toluene (20 mL) were added subsequently. The mixture was refluxed overnight under nitrogen. The reaction mixture was quenched by saturated aqueous ammonium chloride solution and extracted with ethyl acetate (3 × 10 mL). The combined organic layers were washed with brine water and then dried over anhydrous magnesium sulfate, filtered, and concentrated in vacuo to give the crude product, which was purified by column chromatograph packed with silica gel using petroleum ether/dichloromethane (10:1 to 3:1) as eluent to afford a green–yellow oil (852 mg, 54% yield). IR (KBr): 2957, 2922, 2855, 1506, 1282, 1074, 430 cm^{-1}. ^1H NMR (400 MHz, $CDCl_3$): δ 8.35 (d, J = 7.6 Hz, 1H), 8.29 (d, J = 7.4 Hz, 1H), 8.16 (d, J = 8.6 Hz, 1H), 7.59 (d, J = 8.8 Hz, 2H), 7.45–7.41 (m, 2H), 7.40–7.32 (m, 5H), 7.21 (d, J = 7.1 Hz, 1H), 7.16 (d, J = 7.0 Hz, 2H), 7.12 (d, J = 8.8 Hz, 2H), 7.02 (dd, J = 8.6 Hz, J = 2.1 Hz, 1H), 6.87 (d, J = 7.0 Hz, 2H), 4.31–4.28 (m, 2H), 4.25–4.23 (m, 2H), 3.97 (t, J = 6.5 Hz, 2H), 2.98–2.83 (m, 6H), 2.10–1.97 (m, 4H), 1.93–1.84 (m, 2H), 1.39–1.35 (m, 4H), 1.01–0.80 (m, 42H), 0.68–0.49 (m, 31H). ^{13}C NMR (100 MHz, $CDCl_3$): δ 155.8, 155.0, 153.6, 146.8, 146.2, 144.6, 144.0, 142.2, 140.5, 140.4, 138.3, 138.2, 138.1, 137.3, 134.8, 133.2, 130.9, 128.8, 128.6, 127.1, 126.8, 126.6, 126.5, 126.2, 126.0, 125.9, 125.3, 124.6, 122.4, 122.2, 121.2, 117.1, 116.9, 115.3, 97.6, 96.5, 68.3, 65.6, 64.8, 64.5, 55.6, 55.5, 37.0, 36.8, 31.9, 31.6, 31.5, 30.6, 30.3, 30.2, 29.7, 29.5, 29.4, 25.8, 24.0, 23.9, 23.8, 22.7, 22.6, 22.4, 22.3, 22.2, 19.2, 14.1, 14.0, 13.9, 13.7. HRMS (ESI) calcd for $C_{87}H_{115}NO_3S$ ($M + H^+$): 1254.8676, found: 1254.8673.

4.4.4. Synthesis of compound **6**

$POCl_3$ (169 mg, 1.1 mmol) was added dropwisely into dry DMF (3 mL) at 0 °C. The reaction was stirred at 0 °C for 30 min and a solution of compound **5** (1254 mg, 1.0 mmol) in dry DMF (5 mL) was added via a syringe. After the addition, the mixture was stirred overnight at room temperature. Ice water was added to terminate the reaction, and the product was extracted with ethyl acetate (3 × 10 mL). The combined organic layers were washed with brine and then dried over anhydrous magnesium sulfate, filtered, and concentrated in vacuo to give the crude product, which was purified by column chromatograph packed with silica gel using petroleum ether/dichloromethane (10:1 to 2:1) to give the desired aldehyde **6** (1089 mg, 85% yield). IR (KBr): 3446, 2958, 2926, 2856, 1726, 1647, 1442, 1281, 1076, 463 cm^{-1}. ^1H NMR (400 MHz, $CDCl_3$): δ 9.91 (s, 1H), 8.35 (d, J = 7.6 Hz, 1H), 8.28 (d, J = 7.4 Hz, 1H), 8.20 (d, J = 8.6 Hz, 1H), 7.66 (d, J = 7.1 Hz, 2H), 7.46–7.42 (m, 2H), 7.40–7.34 (m, 4H), 7.24 (m, 1H), 7.16 (d, J = 7.1 Hz, 2H), 7.10 (d, J = 8.8 Hz, 2H), 7.06 (dd, J = 8.6 Hz, J = 2.1 Hz, 1H), 6.89 (d, J = 8.8 Hz, 2H), 4.42–4.40 (m, 2H), 4.37–4.35 (m, 2H), 3.98 (t, J = 6.5 Hz, 2H), 2.98–2.84 (m, 6H), 2.10–2.00 (m, 4H), 1.94–1.84 (m, 2H), 1.40–1.34 (m, 4H), 0.99–0.84 (m, 42H), 0.66–0.46 (m, 31H). ^{13}C NMR (100 MHz, $CDCl_3$): δ 179.3, 167.7, 156.3, 155.2, 153.6, 153.5, 149.1, 148.9, 145.5, 144.6, 144.3, 144.2, 140.4, 140.3, 139.8, 138.4, 138.3, 138.0, 136.8, 135.8, 132.4, 130.9, 129.8, 128.8, 127.8, 127.5, 127.0, 126.3, 125.9, 125.4, 124.6, 124.5, 124.0, 122.2, 122.1, 121.0, 117.9, 115.5, 114.6, 68.4, 65.5, 65.1, 64.5, 55.6, 55.5, 37.0, 36.8, 31.6, 31.5, 31.4, 30.6, 29.7, 29.4, 29.3, 25.8, 24.0, 23.9, 23.8, 22.6, 22.3, 22.2, 19.2, 14.0, 13.9, 13.8, 13.7. HRMS (ESI) calcd for $C_{88}H_{115}NO_4S$ ($M + H^+$): 1282.8625, found: 1282.8610.

4.4.5. Synthesis of M24

To a stirred solution of aldehyde **6** (256 mg, 0.2 mmol) and cyanoacetic acid (26 mg, 0.3 mmol) in acetonitrile (8 mL) was added chloroform (4 mL) and piperidine (50 μL). The reaction mixture was refluxed for 8 h. Additional cyanocertic acid (0.2 mmol) and piperdine (50 μL) were added. The mixture was refluxed for another 8 h and then acidified with 1 M hydrochloric acid aqueous solution (30 mL). The crude product was extracted with CH_2Cl_2 (3 × 10 mL). The combined organic layers were washed with brine and then dried over anhydrous magnesium sulfate, filtered, and concentrated in vacuo to give the crude product. The residue was purified by column chromatography packed with silica gel using CH_2Cl_2/CH_3OH (50:1 to 10:1) as eluent to give a red power (202 mg, 75% yield). Mp: 179–180 °C. IR (KBr): 3441, 2924, 2856, 1628, 1571, 1447, 1237, 1069, 748 cm^{-1}. ^1H NMR (400 MHz, $CDCl_3$): δ 8.43 (s, 1H), 8.36 (d, J = 7.6 Hz, 1H), 8.30 (d, J = 7.4 Hz, 1H), 8.23 (d, J = 8.6 Hz, 1H), 7.72 (d, J = 8.4 Hz, 2H), 7.46–7.43 (m, 2H), 7.40–7.33 (m, 4H), 7.25 (m, 1H), 7.17 (d, J = 8.4 Hz, 2H), 7.11–7.08 (m, 3H), 6.90 (d, J = 8.8 Hz, 2H), 4.42–4.30 (m, 4H), 3.99 (t, J = 6.5 Hz, 2H), 2.96–2.84 (m, 6H), 2.11–2.00 (m, 4H), 1.96–1.88 (m, 2H), 1.37–1.35 (m, 4H), 1.01–0.86 (m, 42H), 0.72–0.51 (m, 31H). ^{13}C NMR (100 MHz, $CDCl_3$): δ 168.6, 167.7, 163.2, 156.4, 155.3, 153.6, 153.5, 149.6, 149.2, 145.3, 144.7, 144.4, 144.2, 142.2, 140.4, 140.2, 139.6, 138.4, 138.3, 138.0, 136.9, 136.0, 132.4, 131.5, 130.9, 129.0, 128.8, 128.2, 127.6, 126.3, 126.0, 125.4, 124.6, 123.6, 122.4, 122.2, 120.6, 118.1, 117.0, 115.5, 109.6, 91.8, 68.4, 65.6, 65.4, 64.5, 58.5, 55.7, 55.6, 55.5, 48.0, 37.0, 36.8, 36.7, 36.1, 34.7, 31.9, 31.7, 31.6, 31.5, 31.4, 30.6, 30.3, 29.7, 29.6, 29.4, 29.3, 29.1, 25.8, 24.0, 23.8, 22.8, 22.7, 22.6, 22.5, 22.3, 22.2, 19.2, 18.3, 14.1, 14.0, 13.9, 13.8, 13.7. HRMS (ESI) calcd for $C_{91}H_{116}N_2O_5S$ ($M + H^+$): 1350.8716, found: 1350.8695.

Acknowledgments

We gratefully acknowledge the financial support from the National MOST (2011CBA00702), National Natural Science Foundation of China (21373007, 21376179) and the Tianjin Natural Science Foundation (13JCZDJC32400).

References

[1] B. O'Regan, M. Grätzel, Nature 353 (1991) 737–740.
[2] (a) M.K. Nazeeruddin, F. De Angelis, S. Fantacci, A. Selloni, G. Viscardi, P. Liska, S. Ito, B. Takeru, M.G. Grätzel, J. Am. Chem. Soc. 127 (2005) 16835–16847;
(b) M. Grätzel, J. Photochem. Photobiol. C Photochem. Rev. 4 (2003) 145–153.
[3] A. Hagfeldt, G. Boschloo, L. Sun, L. Kloo, H. Pettersson, Chem. Rev. 110 (2010) 6595–6663.
[4] (a) W.D. Zeng, Y.M. Cao, Y. Bai, Y.H. Wang, Y.S. Shi, M. Zhang, F.F. Wang, C.Y. Pan, P. Wang, Chem. Mater. 22 (2010) 1915–1925;
(b) M. Zhang, Y. Wang, M. Xu, W. Ma, R. Li, P. Wang, Energy Environ. Sci. 6 (2013) 2944–2949.
[5] (a) Z.-S. Wang, N. Koumura, Y. Cui, M. Takahashi, H. Sekiguchi, A. Mori, T. Kubo, A. Furube, K. Hara, Chem. Mater. 20 (2008) 3993–4003;
(b) Q. Feng, G. Zhou, Z.-S. Wang, J. Power Sources 239 (2013) 16–23.
[6] R. Chen, X. Yang, H. Tian, X. Wang, A. Hagfeldt, L. Sun, Chem. Mater. 19 (2007) 4007–4015.
[7] W. Zhu, Y. Wu, S. Wang, W. Li, X. Li, J. Chen, Z.-S. Wang, H. Tian, Adv. Funct. Mater. 21 (2011) 756–763.
[8] Z.J. Ning, Y. Fu, H. Tian, Energy Environ. Sci. 3 (2010) 1170–1181.
[9] (a) Y. Liang, B. Peng, J. Liang, Z. Tao, J. Chen, Org. Lett. 12 (2010) 1204–1207;
(b) M. Liang, W. Xu, F. Cai, P. Chen, B. Peng, J. Chen, Z. Li, J. Phys. Chem. C 111 (2007) 4465–4472.
[10] J. Chang, C.-P. Lee, D. Kumar, P.-W. Chen, L.-Y. Lin, K.R. Justin Thomas, K.-C. Ho, J. Power Sources 240 (2013) 779–785.
[11] Y. Hua, S. Chang, H. Wang, D. Huang, J. Zhao, T. Chen, W.-Y. Wong, W.-K. Wong, X. Zhu, J. Power Sources 243 (2013) 253–259.
[12] T. Duan, K. Fan, C. Zhong, X. Chen, T. Peng, J. Qin, J. Power Sources 234 (2013) 23–30.
[13] B. Liu, W. Li, B. Wang, X. Li, Q. Liu, Y. Naruta, W. Zhu, J. Power Sources 234 (2013) 139–146.
[14] G. Wu, F. Kong, J. Li, X. Fang, Y. Li, S. Dai, Q. Chen, X. Zhang, J. Power Sources 243 (2013) 131–137.
[15] (a) M. Liang, M. Lu, Q. Wang, W. Chen, H. Han, Z. Sun, S. Xue, J. Power Sources 196 (2011) 1657–1664;
(b) M. Lu, M. Liang, H. Han, Z. Sun, S. Xue, J. Phys. Chem. C 115 (2011) 274–281;
(c) G. Li, M. Liang, H. Wang, Z. Sun, L. Wang, Z. Wang, S. Xue, Chem. Mater. 25 (2013) 1713–1722;
(d) Z. Wang, M. Liang, L. Wang, Y. Hao, C. Wang, Z. Sun, S. Xue, Chem. Commun. 49 (2013) 5748–5750;
(e) Z. Wang, M. Liang, Y. Hao, Y. Zhang, L. Wang, Z. Sun, Song Xue, J. Mater. Chem. A 1 (2013) 11809–11819;
(f) Y. Shi, M. Liang, L. Wang, H. Han, L. You, Z. Sun, S. Xue, ACS Appl. Mater. Interfaces 5 (2013) 144–153.
[16] M. Liang, J. Chen, Chem. Soc. Rev. 42 (2013) 3453–3488.

[17] D. Zhou, Q. Yu, N. Cai, Y. Bai, Y. Wang, P. Wang, Energy Environ. Sci. 4 (2011) 2030–2034.
[18] G. Boschloo, A. Hagfeldt, Acc. Chem. Res. 42 (2009) 1819–1826.
[19] (a) A. Hagfeldt, M. Grätzel, Chem. Rev. 95 (1995) 49–68;
(b) H. Nusbaumer, S.M. Zakeeruddin, J.-E. Moser, M. Grätzel, Chem. Eur. J. 9 (2003) 3756–3763.
[20] S.M. Feldt, E.A. Gibson, E. Gabrielsson, L. Sun, G. Boschloo, A. Hagfeldt, J. Am. Chem. Soc. 132 (2010) 16714–16724.
[21] A. Yella, H.-W. Lee, H.N. Tsao, C. Yi, A.K. Chandiran, M.K. Nazeeruddin, E.W.-G. Diau, C.-Y. Yeh, S.M. Zakeeruddin, M. Grätzel, Science 334 (2011) 629–634.
[22] M. Wang, C. Grätzel, S.M. Zakeeruddin, M. Grätzel, Energy Environ. Sci. 5 (2012) 9394–9405.
[23] Y.M. Cao, N. Cai, Y.L. Wang, R.Z. Li, Y. Yuan, P. Wang, Phys. Chem. Chem. Phys. 14 (2012) 8282–8286.
[24] L.E. Polander, A. Yella, J. Teuscher, R. Humphry-Baker, B.F.E. Curchod, N.A. Astani, P. Gao, J.-E. Moser, I. Tavernelli, U. Rothlisberger, M. Grätzel, M.K. Nazeeruddin, J. Frey, Chem. Mater. 25 (2013) 2733–2739.
[25] X.P. Zong, M. Liang, C.R. Fan, K. Tang, G. Li, Z. Sun, S. Xue, J. Phys. Chem. C 116 (2012) 11241–11250.
[26] X.P. Zong, M. Liang, T. Chen, J.N. Jia, L.N. Wang, Z. Sun, S. Xue, Chem. Commun. 48 (2012) 6645–6647.
[27] (a) Z. Ning, Q. Zhang, H. Pei, J. Luan, C. Lu, Y. Cui, H. Tian, J. Phys. Chem. C 113 (2009) 10307–10313;
(b) K. Do, D. Kim, N. Cho, S. Paek, K. Song, J. Ko, Org. Lett. 14 (2012) 222–225;
(c) S. Wang, J. Guo, L. He, H. Wang, J. Zhao, C. Lu, Synth. Met. 168 (2013) 1–8.
[28] M.K. Kashif, J.C. Axelson, N.W. Duffy, C.M. Forsyth, C.J. Chang, J.R. Long, L. Spiccia, U. Bach, J. Am. Chem. Soc. 134 (2012) 16646–16653.
[29] X.F. Wang, H. Tamiaki, L. Wang, N. Tamai, O. Kitao, H.S. Zhou, S.I. Sasaki, Langmuir 26 (2010) 6320–6327.
[30] N.W. Duffy, L.M. Peter, R.M.G. Rajapakse, K.G.U. Wijayantha, J. Phys. Chem. B 104 (2000) 8916–8919.
[31] (a) G. Schlichthörl, S.Y. Huang, J. Sprague, A.J. Frank, J. Phys. Chem. B 101 (1997) 8141–8155;
(b) G. Schlichtho1rl, N.G. Park, A.J. Frank, J. Phys. Chem. B 103 (1999) 782–791.
[32] S.E. Koops, B.C. O'Regan, P.R.F. Barnes, J.R. Durrant, J. Am. Chem. Soc. 131 (2009) 4808–4818.